THE JOURNAL OF PHYSICAL CHEMISTRY C

Article

pubs.acs.org/JPCC

Reactions of CO, H_2O, CO_2, and H_2 on the Clean and Precovered Fe(110) Surfaces − A DFT Investigation

Shaoli Liu,[†,‡,§] Yong-Wang Li,*[,†,‡] Jianguo Wang,[†] and Haijun Jiao*[,†,∥]

[†]State Key Laboratory of Coal Conversion, Institute of Coal Chemistry, Chinese Academy of Sciences, Taiyuan, 030001, China

[‡]National Energy Center for Coal to Liquids, Synfuels China Co., Ltd., Huairou District, Beijing, 101400, China

[§]University of Chinese Academy of Sciences, No. 19A Yuquan Road, Beijing, 100049, P. R. China

[∥]Leibniz-Institut für Katalyse e.V. an der Universität Rostock, Albert-Einstein Strasse 29a, 18059 Rostock, Germany

Supporting Information

ABSTRACT: The reactions of CO and H_2O on the clean Fe(110) surface as well as surfaces with 0.25 monolayer O, OH, and H precoverage have been computed on the basis of density functional theory (GGA-PBE). Under the considerations of the reductive nature of CO as reactant and H_2 as product as well as the oxidative nature of CO_2 and H_2O, we have studied the potential activity of metallic iron in the water-gas shift reaction. On the clean surface, CO oxidation following the redox mechanism has a similar barrier as CO dissociation; however, CO dissociation is much more favorable thermodynamically. Furthermore, surfaces with 0.25 monolayer O, OH, and H precoverage promote CO hydrogenation, while they suppress CO oxidation and dissociation. On the surfaces with different CO and H_2O ratios, CO hydrogenation is promoted. On all of these surfaces, COOH formation is not favorable. Considering the reverse reaction, CO_2 dissociation is much favorable kinetically and thermodynamically on all of these surfaces, and CO_2 hydrogenation should be favorable. Finally, metallic iron is not an appropriate catalyst for the water-gas shift reaction.

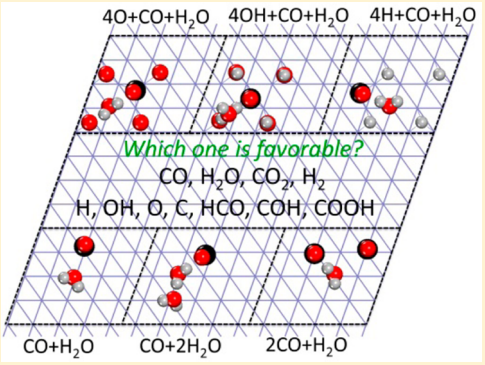

1. INTRODUCTION

Small molecules like CO, H_2, CO_2, and H_2O are very important and useful basic chemicals and have found wide applications in many practical industrial processes for the production of large-scale chemicals. Among all of these reactions, the water-gas shift (WGS) reaction [$CO(g) + H_2O(g) = CO_2(g) + H_2(g)$; $\Delta H = -41.1$ kJ/mol], which involves all of these four basic chemicals, has been widely used for H production in the fertilizer industry and petroleum refinery for a variety of operations as well as in energy society.[1,2] Because of its kinetic limitation and reversibility,[1] the WGS reaction is thermodynamically favored at low temperature, while kinetically favored at high temperature, and therefore, the WGS reaction is typically carried out in two steps: high-temperature operation to convert CO and low-temperature operation to achieve lower CO content.[1,3−5] Low-temperature WGS reaction plays an important role in many industrial processes such as methanol synthesis, methanol steam reforming, catalytic combustion, Fischer−Tropsch synthesis, and cleaning of H_2 stream from CO prior to feeding H_2 to low-temperature fuel cells.[6]

The WGS reaction can be catalyzed by metals and metal oxides. It is reported that iron oxide/chromium oxide catalysts could work only at high temperature,[1] and copper-based catalysts could operate at low temperatures. Although the WGS reaction looks simple, its detailed mechanisms are still not fully understood on various surfaces. Experimentally, the mechanisms of the WGS reaction catalyzed by Co,[7−9] Fe,[7,8,10] Ni,[7,8,10−12] Ru,[11,13] Rh,[11−14] Pd,[7,8,11−13,15−17] and Pt[3,11−15,18−21] supported on metal oxides (Fe_2O_3, TiO_2, CeO_2, La_2O_3, Al_2O_3, MgO, MoS_2, and SiO_2), as well as metal sulfide and carbides, such as MoS_2[9,10] and Mo_2C,[22,23] have been extensively studied. There are many theoretical studies on the mechanisms of the WGS reaction catalyzed by metallic catalysts [Cu,[24,25] Pt,[5,6] Au,[26−29] and Ag[29]] and metal/oxide catalysts [Cu/CeO_2,[30] Au/CeO_2,[30] Cu/ZnO,[30] Au/ZnO,[30] Cu/TiO_2,[31] Au/TiO_2,[31] Cu/ZrO_2,[32] CeOx/Cu,[33] $Au/CeO_x/TiO_2$,[34] $Cu/CeO_x/TiO_2$,[34] and $Pt/CeO_x/TiO_2$[34]].

Two typical WGS reaction mechanisms have often been proposed, i.e., the regenerative redox mechanism[7,11,14,16,17,20,35] and the intermediate-mediated mechanism.[6,8,18,21,32] The redox mechanism features the elementary steps of $H_2O^* \rightarrow O^* + H_2(g)$ and $CO^* + O^* \rightarrow CO_2 + 2^*$ (an asterisk for a surface vacant site). This mechanism involves the steps of CO and H_2O adsorption (R1 and R2) and H_2O dissociation (R3, R4, and R5) as well as the formation and desorption of CO_2 (R6 and R7) and H_2 (R8). The reported rate-limiting steps in the mechanism are water activation and CO oxidation.[7,11,14,16,17,20,35]

Received: August 3, 2015
Revised: November 26, 2015
Published: November 30, 2015

DOI: 10.1021/acs.jpcc.5b07497
J. Phys. Chem. C 2015, 119, 28377−28388

$$H_2O(g) + * \rightarrow H_2O* \quad (R1)$$

$$CO(g) + * \rightarrow CO* \quad (R2)$$

$$H_2O + * \rightarrow OH* + H* \quad (R3)$$

$$OH* + * \rightarrow O* + H* \quad (R4)$$

$$2OH* + * \rightarrow O* + H_2O* \quad (R5)$$

$$CO + O* \rightarrow CO_2* + * \quad (R6)$$

$$CO_2* \rightarrow CO_2 + * \quad (R7)$$

$$2H* \rightarrow H_2 + * \quad (R8)$$

The intermediate-mediated mechanism involves the carbon-containing intermediates (formate and carboxyl), which are formed via the coupling of CO and surface species (H and OH). In the carboxyl-intermediate (COOH) mechanism, the reaction involves COOH formation (R9) and dissociation (R10−R12) along with the steps in the redox mechanism.[6,24]

$$CO + OH* \rightarrow COOH* + * \quad (R9)$$

$$COOH* + * \rightarrow CO_2* + H* \quad (R10)$$

$$COOH* + O* \rightarrow CO_2* + OH* \quad (R11)$$

$$COOH* + OH* \rightarrow CO_2* + H_2O* \quad (R12)$$

In the formate-intermediate (HCOO) mechanism, the reaction mechanism involves the direct (R13) and mediated (R14 and R15) dissociation of surface HCOO along with the steps in the redox mechanism.[6] In fact, the formation of HCOO from CO and OH would involve several bond-breaking and bond-forming steps, which might involve large activation energy barriers. It is proposed that the formation of HCOO comes from the coupling of CO_2 and surface H atom[9,10] and such coupling reaction can be rationalized from the aspect of the frontier molecular orbitals of the CO_2 and H atom. Previous studies reported that the HCOO is a spectator only and not involved in the WGS reaction mechanism.[6,14,16,20,24]

$$HCOO* + * \rightarrow CO_2* + H* \quad (R13)$$

$$HCOO* + O* \rightarrow CO_2* + OH* \quad (R14)$$

$$HCOO* + OH* \rightarrow CO_2* + H_2O* + * \quad (R15)$$

Iron oxide catalysts are called high-temperature shift catalysts, and there are many investigations about the WGS reaction on iron oxide catalysts.[36−46] Generally, Fe_3O_4 is thought to be the active component in iron-based catalysts. However, Fe_3O_4 can sinter rapidly and lose its activity at high temperature.[46] Recently, dopants, such as Cr,[2,1,38] Ce,[47] Zn,[48] La,[49] and Cu,[46,50] were added to iron-based catalysts for improving the performance and efficiency. Despite wide industrial applications as well as experimental and theoretical investigations, the mechanisms of the WGS reaction catalyzed by Fe_3O_4 are still not well understood.

Considering the reductive nature of CO and H_2 as reactants, one might guess the components of the Fe-based catalysts. For example, do the catalysts only have Fe_3O_4 as the active component or can metallic iron formed from Fe_3O_4 reduction be the active component? Indeed, there is experimental evidence that metallic iron is present under the real FTS reaction conditions and also considered as active catalyst for the FTS reaction. For example, using Mössbauser spectroscopy, X-ray diffraction, carbon content determination, and reaction kinetic measurements, Niemantsverdriet et al.[51] studied the conversion of metallic iron catalysts into carbides. Under the condition of $T < 513$ K, they found α-Fe as the main phase. In a widely accepted view of the iron catalyst, Dry[52] showed that, at the start of the FTS reaction, the catalyst is predominantly in the form of metallic iron, which is converted to Fe_3O_4 and iron carbides; however, even after a long time-on-stream, there is still metallic iron present in the catalyst. Dictor et al.[53] reported that the active phase in the FTS reaction is a mixture of χ- and ϵ'-carbides and some metallic α-Fe. Eliason et al.[54] reported the rate data for the FTS reaction on unsupported Fe and Fe/K catalysts and found that, on Fe catalysts, the FTS reaction mechanisms can be expressed by a sequence of elementary steps, including H_2 dissociative adsorption, molecular and dissociative adsorption of CO, hydrogenation of atomic carbon to CH_x species, polymerization of CH_x species to hydrocarbons, and formation of CO_2 from CO and O. Lohitharn et al.[55] studied the effect of transition-metal promoters for the Fe-based FTS catalysts and found that metallic iron has catalytic activity in CO hydrogenation, although it is lower. Ojeda et al.[56] studied CO activation pathways and FTS mechanisms on the Fe(110) surface and found that the preferred CO dissociation pathway is H-assisted with CH formation through deoxygenation reaction.

On the basis of this experimental evidence, we carried out a systematic density functional theory (DFT) study to investigate the mechanism of the WGS reaction on the metallic Fe(110) surface. The reaction mechanisms, including redox and COOH- and COH- as well as the HCO-mediated steps, have been examined. We also considered the reaction pathways under different conditions, such as on the O-, OH-, and H-precovered surfaces as well as different H_2O/CO ratios.

2. METHODS AND MODELS

2.1. Method. All calculations were performed with the plane-wave pseudopotential code in the Vienna Ab initio Simulation Package (VASP).[57,58] The electron−ion interaction is described with the projector augmented wave (PAW)[59,60] method. Exchange and correlation energies were described using the spin-polarized generalized gradient approximation and Perdew−Burke−Ernzerhof functional (GGA-PBE).[61] Spin-polarized calculations were performed to account for the magnetic properties of iron. Transition-state structures were estimated by using the climbing image nudged elastic band method (CI-NEB).[62] For each optimized stationary state, vibrational analysis was performed at the same level of theory to determine its character as either minimum or saddle point. The optimized lattice parameter was calculated using the body-centered cubic (bcc) unit cell, and its reciprocal space is sampled with a 15 × 15 × 15 k-point grid generated automatically using the Monkhorst−Pack method.[63] The optimized lattice constant is close to the experimental value (2.835 vs 2.866 Å[64]). The calculated magnetic moment is close to the experimental value (2.226 vs 2.22 μ_B[65]). Our previous studies showed that PBE is very well applicable in studying the adsorption, dissociation, and desorption of H_2O,[66−68] H_2,[69] and CO[70,71] on different Fe surfaces, while dispersion correction for counting van der Waals interaction (PBE-D2) very often overestimates the adsorption strength of these systems.

2.2. Model. For the Fe(110) surface, a periodic slab with a vacuum region 15.0 Å in width was used to separate the repeating slabs. We used the same model as reported

DOI: 10.1021/acs.jpcc.5b07497
J. Phys. Chem. C 2015, 119, 28377−28388

previously.[67] The surface structural relaxation and the total energy calculation were performed with 3 × 3 × 1 Monkhorst−Pack *k*-point sampling. The $p(4 \times 4)$ surface size was used. A four-layer model was used, where the first two layers including adsorbates were relaxed and the bottom two layers were fixed. The structure includes 64 Fe atoms. The top and side views and possible adsorption sites of the Fe(110) surface are shown in Figure 1. We considered the top (**T**), long-bridge (**LB**), short-bridge (**SB**), and 3-fold-hollow (**3FH**) sites of the Fe(110) surface. The choice of the Fe(110) facet as a model is based on the fact that the Fe(110) facet is the most exposed facet from Fe_2O_3 under H_2 reduction atmosphere,[72] and this is also confirmed by ab initio thermodynamics on the basis of surface free energies.[70]

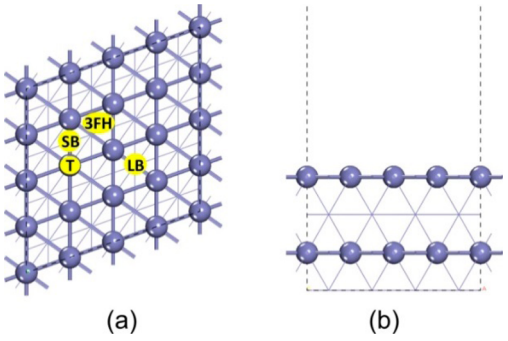

Figure 1. Top (a) and side (b) views of the Fe(110) surface structures with possible adsorption sites: top (**T**), long-bridge (**LB**), short-bridge (**SB**), and 3-fold-hollow (**3FH**) sites.

The adsorption energy (E_{ads}) was calculated by using the expression defined as $E_{ads} = E_{X/slab} - E_{slab} - E_X$, where $E_{X/slab}$ is the total energy of the slab with adsorbed molecules in its equilibrium geometry, E_{slab} is the total energy of the clean surface, and E_X is the total energy of the free adsorbates in gas phase. Therefore, the more negative the E_{ads}, the stronger the adsorption. The barrier (E_a) and the reaction energy (E_r) are calculated according to $E_a = E_{TS} - E_{IS}$ and $E_r = E_{FS} - E_{IS}$, where E_{IS}, E_{TS}, and E_{FS} are the energies of the corresponding initial state (IS), transition state (TS), and final state (FS), respectively. It is noted that the reported energies do not include the corrections of zero-point energies (E_{ads}), since they have little effect on the surface reaction and mainly affect the gas molecules.[69,71,73]

3. RESULTS AND DISCUSSION

In this section, we described the WGS reaction including the redox and COOH-, HCO-, and COH-mediated mechanisms on different surfaces, such as on the OH-, O-, and H-precovered surfaces at a given coverage, as well as with different H_2O/CO ratios. We computed all possible parallel and competitive routes, and the results have been summarized in potential energy surface (PES). We considered several possible and logical adsorbed geometries and searched several reaction paths. In this work, the reactions of CO and H_2O on all the considered surfaces are the most favorable paths among these possibilities.

3.1. Adsorption of CO, CO_2, HCO, COH, COOH, and HCOO. In our previous study,[67] the adsorption of H, O, OH, and H_2O on the clean Fe(110) surface has been described in detail. Here, we only considered the adsorption of the reactants, intermediates, and products involved in the WGS reaction on the basis of their most stable positions (Figure 2). The adsorption energies and the selected bond lengths of the corresponding structures are listed in Table 1.

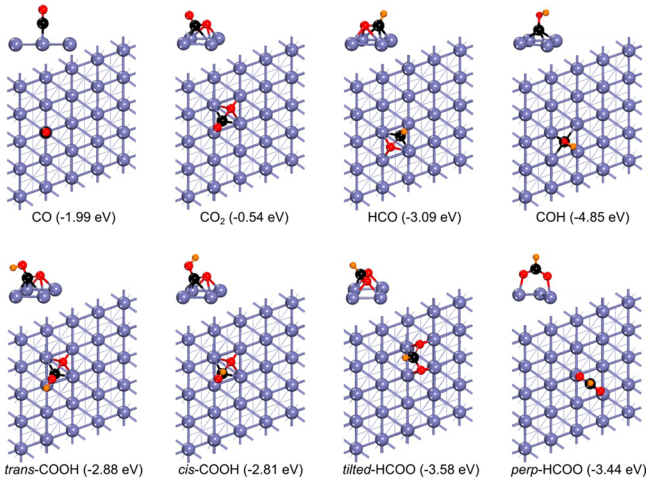

Figure 2. Adsorption configurations and energy of CO, CO_2, HCO, COH, COOH, and HCOO on Fe(110).

3.1.1. CO and CO_2 Adsorption. As found in previous studies,[73−77] the most stable CO adsorption configuration is at the **T** site with the C atom binding to the surface iron atom, and the distances of Fe−C and C−O are 1.769 and 1.174 Å, respectively. Our calculated adsorption energy (−1.99 eV) is close to the available data with PW91 (−1.95 eV)[74] and PBE (−1.88[73,75,77] and −2.00 eV[76]). We also calculated the stable configurations at the **LB** (−1.94 eV) and **3FH** (−1.94 eV) sites, and the adsorption energies are very close to that at the **T** site, indicating the possibility and flexibility of CO adsorption.

In the most stable CO_2 adsorption configuration, CO_2 adsorbs crossing the **LB** site over two **3FH** sites in a bent way, where the C atom is at one **3FH** site with the Fe−C distances of 1.972, 2.260, and 2.261 Å, and one O atom is at the neighboring **3HF** site with the Fe−O distances of 2.037, 2.211, and 2.212 Å, while the second O atom is pointing away from the surface with the OCO angle of 125.8°. The computed C−O bond lengths are 1.232 and 1.369 Å. The computed adsorption energy is −0.54 eV, in agreement with the previous study (−0.56 eV/PBE).[78]

3.1.2. HCO and COH Adsorption. In the most stable HCO adsorption configuration, HCO adsorbs crossing the **LB** site over two **3FH** sites in a bent way, where the C atom is at one **3FH** site with the Fe−C distances of 1.932, 2.105, and 2.176 Å, and the O atom is at the neighboring **3HF** site with the Fe−O distances of 2.020, 2.131, and 2.267 Å, while the H atom is pointing away from the surface with the HCO angle of 112.3°. The computed adsorption energy is −3.09 eV, and the computed C−O and C−H distances are 1.353 and 1.107 Å, respectively.

In the most stable COH adsorption configuration, COH adsorbs crossing the **LB** site with the Fe−C distances of 1.894, 1.896, 2.210, and 2.246 Å. The C−O bond sites are perpendicular to the iron surface, the C−O distance is 1.358 Å, and the O−H bond is nearly parallel to the iron surface. The computed adsorption energy is −4.85 eV. In the gas phase, the HCO radical is more stable than the COH radical by 1.83 eV, and this is governed by the 5σ lone pair of the carbon atom in the highest occupied orbital of the CO molecule. On the

DOI: 10.1021/acs.jpcc.5b07497
J. Phys. Chem. C 2015, 119, 28377−28388

Table 1. Adsorption Energies (E_{ads}, eV) and Relevant Distances (d, Å) of CO, CO_2, HCO, COH, COOH, and HCOO on Fe(110)

	E_{ads}	d_{Fe-C}	d_{Fe-O}	d_{C-O}	d_{C-H}	d_{O-H}
CO	−1.99	1.769		1.174		
CO_2	−0.54	1.972; 2.260; 2.261	2.037; 2.211; 2.212	1.232; 1.369		
HCO	−3.09	1.932; 2.105; 2.176	2.020; 2.131; 2.267	1.353	1.107	
COH	−4.85	1.894; 1.896; 2.210; 2.246		1.358		0.982
trans-COOH	−2.88	1.936; 2.236; 2.274	2.294; 2.135; 2.212	1.334; 1.355		0.982
cis-COOH	−2.81	1.943; 2.247; ;2.267	2.090; 2.211; 2.224	1.342; 1.353	1.097	0.986
tilted-HCOO	−3.58	2.158; 2.411	2.009; 2.037; 2.024; 2.041	1.344; 1.345	1.099	
perp-HCOO	−3.44		1.977; 1.980	1.272; 1.273	1.105	

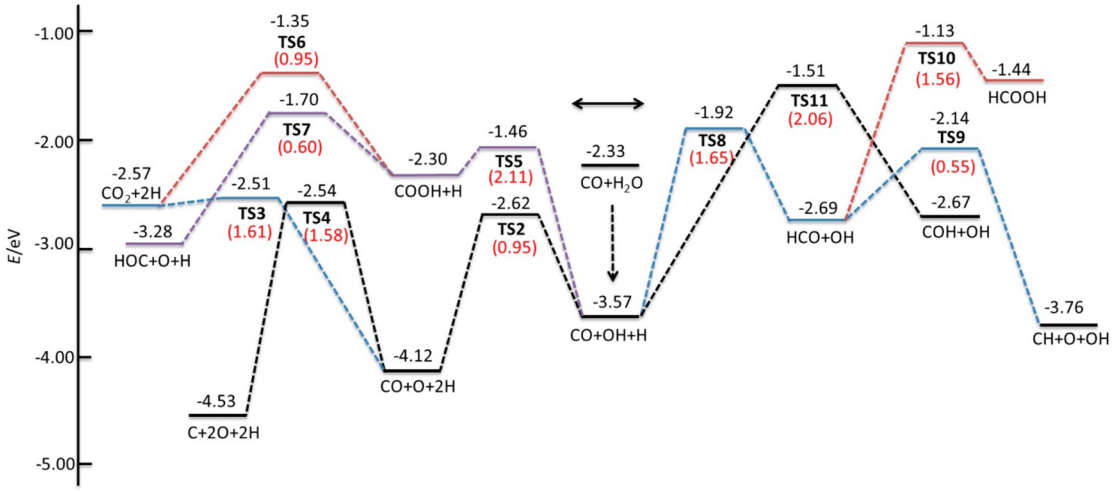

Figure 3. Potential energy surfaces of the reactions of CO and H_2O on the clean Fe(110) surface.

Fe(110) surface, the adsorbed HCO species is more stable than the adsorbed COH species by only 0.07 eV, indicating that, on the surface, from CO hydrogenation, both HCO and COH could be possible thermodynamically.

3.1.3. COOH and HCOO Adsorption. For COOH, there exist two stable adsorption configurations on the basis of the bent CO_2. In the first one, COOH has a *trans*-conformation with the O−H bond pointing toward to the surface, the C−O distances are 1.334 and 1.355 Å, and the adsorption energy is −2.88 eV. In the second one, COOH has a *cis*-conformation with the O−H bond pointing away from the surface, the C−O distances are 1.342 and 1.353 Å, and the adsorption energy is −2.81 eV. In both COOH configurations, the CO_2 unit has the same adsorption configuration and similar structural parameters as only bent CO_2 on the surface (Table 1).

For HCOO, there are also two adsorption configurations, a tilted one and a perpendicular one. In the tilted one, both O atoms are located at the **SB** sites with the Fe−O distances of 2.009, 2.037, 2.024, and 2.041 Å, and the C−H group is tilted over another **SB** site with the Fe−C distances of 2.158 and 2.411 A. The adsorption energy is −3.58 eV. In the perpendicular one, HCOO bridges the **LB** site with the Fe−O distances of 1.977 and 1.980 Å, and the adsorption energy is −3.44 eV. In the gas phase, the COOH radical is more stable than the HCOO radical by 0.39 eV. Adsorbed on the Fe(110) surface, the tilted HCOO is more stable than the *trans*-COOH by 0.29 eV.

3.2. WGS on the Clean Fe(110) Surface. First, we have considered the WGS reaction on the basis of the neighboring adsorbed H_2O + CO on the Fe(110) surface in four competitive pathways. The optimized structures of the IS, TS, and FS are shown in Figures S1−S4, and the structural parameters are listed in Table S1. The reaction barriers, the reaction energies, and the structural parameters of the TS are shown in Table S2. The total reaction PES is shown in Figure 3.

For the neighboring adsorbed H_2O + CO, the adsorption energy is −2.33 eV, which is close to the sum of individual H_2O and CO adsorptions (−2.37 eV). In coadsorbed H_2O + CO, both H_2O and CO are at the top sites and the structural parameters are similar as their individual adsorptions. Within all pathways, the first step is H_2O dissociation and this is because H_2O dissociative adsorption[67] is more favorable kinetically (0.68 vs 1.51 eV) and thermodynamically (−1.28 vs −0.46 eV) than CO direct dissociation on the clean surface.[73] It is also necessary to create surface OH and O to initiate the WGS reaction. In the transition state (**TS1**), the breaking O−H distance is 1.420 Å. In the final state, the adsorbed OH and H are at the **LB** and **3FH** sites, respectively. The energy barrier is 0.70 eV and the reaction is exothermic by 1.24 eV, very similar as that on the clean surface.

3.2.1. Path 1. Since the redox mechanism [CO + OH + H → CO + O + 2H → CO_2 + 2H] needs a surface O atom, we computed surface OH dissociation. In the transition state (**TS2**), the breaking O−H distance is 1.277 Å. In the final state (CO + O + 2H), the O and H atoms are located at the **3FH** sites, and the CO molecule still adsorbs at the top site with the Fe−C distance of 1.771 Å. The computed dissociation barrier is 0.95 eV, and the dissociation is exothermic by 0.55 eV. This is very similar as that on the clean surface (0.90 and −0.57 eV).[67] In addition, it is noted that OH dissociation is more favorable kinetically and thermodynamically than CO dissociation and the surface species should be the coadsorbed CO + O + 2H.

DOI: 10.1021/acs.jpcc.5b07497
J. Phys. Chem. C 2015, 119, 28377−28388

Table 2. Activation Barriers (E_a, eV) and Reaction Energies (E_r, eV) of the Related Elementary Reactions (the Activation Barriers of the Reverse Reaction, $E_{a(r)}$, Are Given in Square Brackets, and Reverse Reaction Energy Is Equal to $-E_r$)

	CO + O → CO_2		CO + H → HCO		CO + OH → COOH		CO → C + O	
	E_a [$E_{a(r)}$]	E_r	E_a [$E_{a(r)}$]	E_r	E_a [$E_{a(r)}$]	E_r	E_a [$E_{a(r)}$]	E_r
Fe(110)	1.61 [0.06]	1.55	1.65 [0.77]	0.88	2.11 [0.84]	1.27	1.58 [1.99]	−0.41
4O/Fe(110)	1.75 [0.44]	1.31	0.67 [0.04]	0.63	1.83 [0.73]	1.10	2.25 [2.12]	0.13
4OH/Fe(110)	1.80 [0.35]	1.45	1.26 [0.27]	0.99	2.04 [0.57]	1.47	2.47 [1.95]	0.52
4H/Fe(110)	1.76 [0.32]	1.44	1.37[a] [0.24[a]]	1.13[a]	1.95 [0.74]	1.21	2.33 [2.70]	−0.37
			1.28[b] [0.66[b]]	0.62[b]				
H_2O/Fe(110)	1.44 [0.49]	0.92	1.44 [0.44]	1.00	2.09 [1.02]	1.07	1.53 [2.02]	−0.49
CO/Fe(110)	1.69 [0.08]	1.61	1.44 [0.72]	0.72	2.14 [0.95]	1.19	1.51 [1.96]	−0.45

[a]From the precovered H. [b]From H after H_2O dissociation.

On the basis of the coadsorbed CO + O + 2H, we computed CO_2 formation [CO + O + 2H → CO_2 + 2H]. In the transition state (**TS3**), the forming C−O distance is 1.657 Å. The computed barrier is 1.61 eV, and CO_2 formation is endothermic by 1.55 eV. This reveals that CO_2 formation is neither kinetically nor thermodynamically favorable, while very easy CO_2 dissociation has been reported.[79] Therefore, the redox mechanism seems very difficult on the Fe(110) surface. In addition, we computed CO direct dissociation from the coadsorbed CO + O + 2H, and it is found that CO direct dissociation has a barrier of 1.58 eV (**TS4**) and is exothermic by 0.41 eV, very similar as that on the clean surface (1.51 and −0.46 eV, respectively).[73] Compared with CO_2 formation, CO dissociation is more favorable thermodynamically by 1.96 eV, and this is because of the very low CO_2 adsorption energy.

3.2.2. Path 2. On the basis of the coadsorbed CO + OH + H, we computed the COOH-mediated reaction [CO + OH + H → COOH + H → CO_2 + 2H]. For COOH formation from CO and OH coupling, the reaction has a barrier of 2.11 eV and is endothermic by 1.27 eV. In the transition state (**TS5**), the forming C−O distance is 1.678 Å. It shows that COOH formation is also very difficult on the Fe(110) surface. Compared with the dissociation of OH and CO, COOH formation is neither kinetically nor thermodynamically favorable.

Nevertheless, we further computed COOH + H dissociation into CO_2 + 2H with the two H atoms adsorbed at the **3FH** sites. In the transition state (**TS6**), the breaking O−H distance is 1.338 Å. The computed barrier is 0.95 eV, and this step is exothermic by 0.27 eV. Alternatively, we also computed COOH dissociation into COH + O. In the transition state (**TS7**), the breaking C−O distance is 1.775 Å. The computed barrier is 0.60 eV, and this step is exothermic by 0.98 eV. This indicates that COOH dissociation into COH + O is more favorable kinetically and thermodynamically than into CO_2 + H. Since COOH formation is very difficult, the COOH route [CO + OH + H → COOH + H → CO_2 + 2H] should also be unlikely.

3.2.3. Path 3. The third path is the HCO-mediated reaction from the coadsorbed CO + OH + H. In the transition state of HCO formation (**TS8**), the forming C−H distance is 1.406 Å, and the energy barrier is 1.65 eV. In the final state, HCO and OH are located at their most stable sites with the Fe−C distances of 1.941, 2.111, and 2.147 Å, and the C−O distance is 1.353 Å. This step is endothermic by 0.88 eV. It is noted that HCO formation is not competitive with OH dissociation kinetically and thermodynamically.

Subsequently, the formed HCO can dissociate into HC and O. In the transition state **TS9**, the breaking C−O distance is 1.821 Å, and this step has an energy barrier of 0.55 eV and is exothermic by 1.07 eV, therefore, favorable kinetically and thermodynamically. Alternatively, the coadsorbed HCO and OH can react to obtain the HCOOH. In the transition state **TS10**, the forming C−O distance is 1.835 Å. However, HCOOH formation is neither kinetically (1.56 eV) nor thermodynamically (1.25 eV) favorable. It is interesting to note that HCOOH dissociation (the back reaction) is very feasible (0.31 and −1.25 eV).

3.2.4. Path 4. The fourth path is the COH-mediated reaction from the coadsorbed CO + OH + H. In the transition state of COH formation (**TS11**), the forming O−H distance is 1.298 Å, and the effective energy barrier is 2.06 eV. In the final state, the COH and OH are located at their most stable sites with the Fe−C distances of 1.868, 1.886, 2.192, and 2.322 Å, and the C−O distance is 1.362 Å. This step is endothermic by 0.90 eV from the stable CO + OH + H. It is not favored both kinetically and thermodynamically. We also do not consider the following steps in this route because of the high barrier and endothermic reaction.

The PES in Figure 3 shows clearly that the most favorable reaction path follows the dissociation of H_2O and CO; and the final surface species is the coadsorbed C + 2O + 2H. With respect to the coadsorbed CO + H_2O, all stationary points of the most favorable reaction path are more stable and the whole dissociation is exothermic by 2.20 eV. Although the redox reaction mechanism [CO + O + 2H → CO_2 + 2H] has a similar barrier as CO dissociation (1.61 vs 1.58 eV), it is much less exothermic by 1.96 eV than CO dissociation.

The PES in Figure 3 and the data listed in Table 2 also show that CO_2 dissociation [CO_2 → CO + O] is much favorable kinetically (nearly barrier-less) and thermodynamically (−1.55 eV); the formed CO can either dissociate [CO → C + O] or be hydrogenated [CO + H → HCO]; and both C and HCO can be further transformed to hydrocarbons.

Since CO direct oxidation and the formation of COOH and COH are not competitive with the dissociative adsorption of H_2O and CO kinetically and thermodynamically, in the following session, we focused on the effect of surface precoverage on CO oxidation as well as the formation of COOH and HCO.

3.3. On 0.25 ML O-Precovered Fe(110) Surface. From surface oxidation via H_2O dissociative adsorption, surface O has saturated coverage of approximately 0.4 ML.[67,80] Since CO dissociation is more favorable than CO_2 formation from CO oxidation thermodynamically, we became interested in the effect of surface oxygen precoverage on the WGS reaction and considered the reaction of CO and H_2O on the most stable 0.25 ML O-precovered Fe(110) surface[67] through the redox and COOH- and HCO-mediated reactions on the basis of 4O

DOI: 10.1021/acs.jpcc.5b07497
J. Phys. Chem. C 2015, 119, 28377−28388

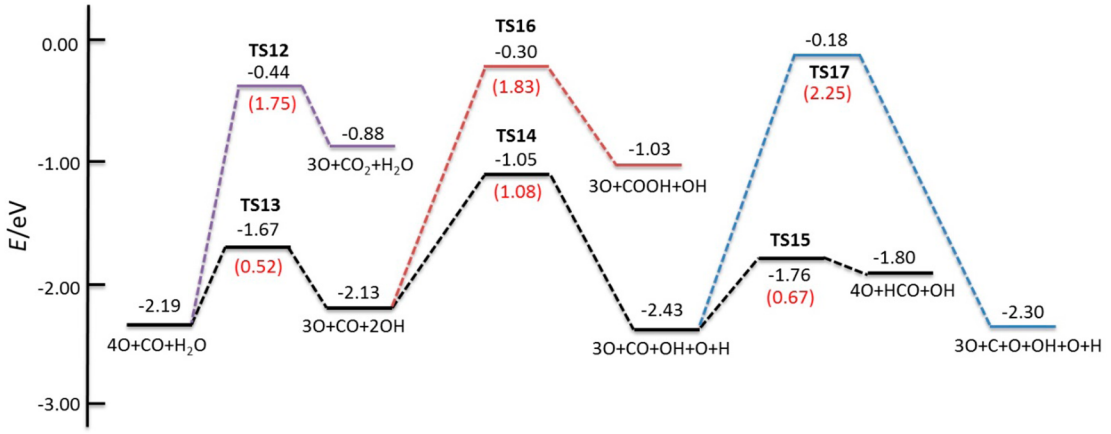

Figure 4. Potential energy surfaces of the reactions of CO and H_2O on the 4O (0.25 ML) precovered Fe(110) surface.

+ CO + H_2O coadsorption. The optimized structures of the IS, TS, and FS are shown in Figure S5, and the structural parameters are listed in Table S3. The reaction barriers, the reaction energies, and the structural parameters of the TS are shown in Table S4. The total reaction PES is shown in Figure 4.

The coadsorption energy of 4O + CO + H_2O is −2.19 eV, which is lower than that (−2.33 eV) on the clean surface. On the coadsorbed 4O + CO + H_2O surface, the adsorbed configurations of H_2O and CO are different from those on the clean surface due to the O precoverage. Although the H_2O molecule still adsorbs at the top site with the Fe−O distance of 2.135 Å, due to the presence of the H-bonding, the H_2O molecule plane has a dihedral angle of 59.1° with the iron surface (vs 14.4° on the clean surface). In addition, CO adsorbs at the **3FH** site with the Fe−C distances of 1.824, 2.159, and 2.198 Å, which are different from the top adsorption configuration on the clean surface. The H-bonding distances between H_2O and O as well as between H_2O and CO are 2.215 and 1.864 Å, respectively.

Although H_2O dissociative adsorption is more favorable, we computed CO direct oxidation to CO_2 [CO + O → CO_2] on the basis of the coadsorbed CO + H_2O + 4O at first. In the transition state **TS12**, the forming C−O distance is 1.768 Å. The energy barrier is 1.75 eV, and the reaction is endothermic by 1.31 eV. This reaction is even more difficult kinetically and thermodynamically than that on the clean surface (1.61 and 0.84 eV), indicating that precovered surface O atoms do not promote CO direct oxidation; instead, precovered surface O atoms might promote CO_2 dissociation. In the final state (3O + CO_2 + H_2O), there is H-bonding between H_2O and CO_2 with the distance of 1.647 Å.

In addition, H_2O and O can react to form 2OH [H_2O + O → 2OH]. In the transition state **TS13**, the breaking and forming O−H distances are 1.313 and 1.129 Å, respectively. This reaction has an energy barrier of 0.52 eV and is endothermic by 0.06 eV. In the final state (3O + CO + 2OH), the two OH species adsorb at the **3FH** sites with the adsorption energy of −2.13 eV.

In the HCO-mediated mechanism [3O + CO + 2OH → 3O + CO + OH + O + H → 4O + HCO + OH], the next step is OH dissociation into O and H atoms. In the transition state **TS14**, the breaking O−H distance is 1.336 Å. OH dissociation has a barrier of 1.08 eV and is exothermic by 0.30 eV. After dissociation, the formed O and H atoms adsorb at the **3FH** site. In the transition state of CO hydrogenation (**TS15**), the forming C−H distance is 1.476 Å. CO hydrogenation has a barrier of 0.67 eV and is endothermic by 0.63 eV. Compared with HCO formation on the clean surface (1.65 and 0.88 eV), CO hydrogenation needs a lower barrier and becomes less endothermic.

In the COOH-mediated mechanism [3O + CO + 2OH → 3O + COOH + OH], the next step is the coupling of OH and CO to form COOH starting from the coadsorbed CO + 2OH + 3O. In the transition state **TS16**, the forming C−O distance is 1.752 Å. The barrier is 1.83 eV, and the reaction is endothermic by 1.10 eV. Compared with that on the clean surface, COOH formation on the O-precovered surface needs a lower barrier and is less endothermic. However, this step is still unfavorable kinetically and thermodynamically.

In addition, we calculated CO direct dissociation into C and O. In **TS17**, the breaking C−O distance is 1.723 Å. The dissociation has a barrier of 2.25 eV and is endothermic by 0.13 eV. Compared with CO dissociation on the clean surface, this reaction is more unfavorable.

The PES in Figure 4 shows clearly that, on the 0.25 ML O (4O) precovered surface, the most favorable route is HCO formation following 4O + CO + H_2O → 3O + CO + 2OH → 3O + CO + OH + O + H → 4O + HCO + OH. With respect to the coadsorbed 4O + CO + H_2O, OH dissociation has the highest barrier (1.14 eV) and HCO formation is endothermic by 0.39 eV. In contrast, CO direct oxidation and COOH formation need much higher barriers (1.75 and 1.89 eV, respectively) and they are also much more endothermic (1.31 and 1.16 eV, respectively).

The PES in Figure 4 shows that CO_2 dissociation [CO_2 → CO + O] is much favorable kinetically (0.44 eV) and thermodynamically (−1.31 eV), and the formed CO can be hydrogenated [CO + H → HCO]. The formed HCO can be further transformed to hydrocarbons.

3.4. On 0.25 ML OH-Precovered Fe(110) Surface. Apart from surface O atoms, surface OH is another principal species, which can be easily formed from either H_2O dissociative adsorption or the reaction with surface O via a very low barrier.[67] Therefore, we investigated the influence of precovered OH species on the WGS reaction on the basis of the 0.25 ML OH-precovered Fe(110) surface. The optimized structures of the stationary points of IS, TS, and FS are shown in Figure S6, and the structural parameters are listed in Table S5. The reaction barriers, the reaction energies, and the structural

DOI: 10.1021/acs.jpcc.5b07497
J. Phys. Chem. C 2015, 119, 28377−28388

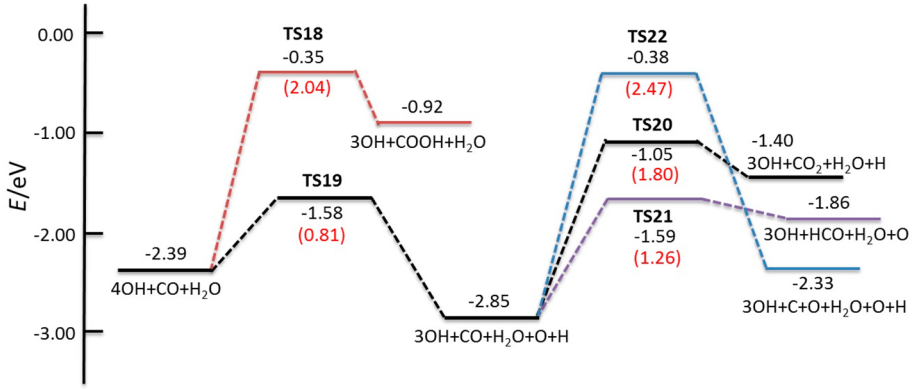

Figure 5. Potential energy surfaces of the reactions of CO and H_2O on the 4OH (0.25 ML) precovered Fe(110) surface.

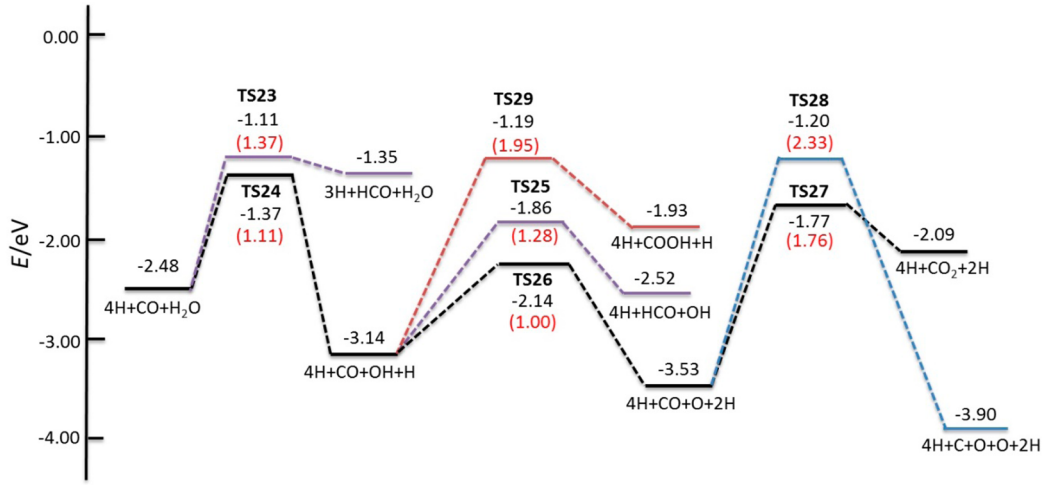

Figure 6. Potential energy surfaces of the reactions of CO and H_2O on the 4H (0.25 ML) precovered Fe(110) surface.

parameters of the TS are shown in Table S6. The total reaction PES is shown in Figure 5.

On the 0.25 ML OH-precovered Fe(110) surface, the coadsorption energy of CO + H_2O is −2.39 eV, which is close to that (−2.33 eV) on the clean surface. In the most stable adsorption configuration, CO adsorbs at the **3FH** site with the Fe−C distances of 1.916, 1.922, and 2.300 Å, and this is different from that on the clean surface at the top site. In addition, H_2O adsorption also differs strongly from that on the clean surface at the top site. The adsorbed H_2O molecule interacts with the surface OH group and CO via the H-bonding between H_2O and OH (1.644 Å) as well as between H_2O and CO (1.786 Å).

Although H_2O dissociative adsorption is more favorable, we computed COOH formation from CO and OH coupling at first. In the transition state of COOH formation (**TS18**), the forming C−O distance is 1.594 Å. COOH formation has a barrier of 2.04 eV and is endothermic by 1.47 eV. In the final state (3OH + COOH + H_2O), the H-bonding between H_2O and OH as well as H_2O and CO is 1.669 and 1.804 Å, respectively. This result indicates that surface OH species can decrease the barrier of COOH formation from CO and OH coupling. However, COOH formation needs a higher barrier and is highly endothermic and is, therefore, unfavorable kinetically and thermodynamically.

Alternatively, one of the OH groups can dissociate into O and H atoms. In the transition state **TS19**, the breaking O−H distance is 1.320 Å. This step needs a barrier of 0.81 eV and is exothermic by 0.46 eV. The formed O and H adsorb at the **3FH** site. The formed O atom can oxidize the CO. In the transition state **TS20**, the forming C−O distance is 1.635 Å. This step needs an effective energy barrier of 1.80 eV and is endothermic by 1.45 eV.

In contrast, the adsorbed CO and H can form HCO starting from the formation of 3OH + CO + H_2O + O + H. In the transition state (**TS21**), the forming C−H distance is 1.539 Å. This step needs an energy barrier of 1.26 eV and is endothermic by 0.99 eV. In the final state (3OH + HCO + H_2O + O), there exists H-bonding between H_2O and OH (1.689 Å) as well as H_2O and HCO (1.812 Å).

In order to compare with the route on the clean surface, we calculated CO direct dissociation into C and O. In the transition state **TS22**, the breaking C−O distance is 1.827 Å. The dissociated barrier is 2.47 eV, and this reaction is endothermic by 0.52 eV. Compared with CO dissociation on the clean surface (1.51 and −0.46 eV, respectively),[73] this reaction becomes less favorable kinetically and thermodynamically.

The PES in Figure 5 shows clearly that, on the 0.25 ML OH-precovered surface, the most favorable reaction is HCO formation following the 4OH + CO + H_2O → 3OH + CO + H_2O + O + H → 3OH + HCO + H_2O + O route, while CO direct oxidation and COOH formation are neither kinetically nor thermodynamically competitive and favorable. Considering

DOI: 10.1021/acs.jpcc.5b07497
J. Phys. Chem. C 2015, 119, 28377−28388

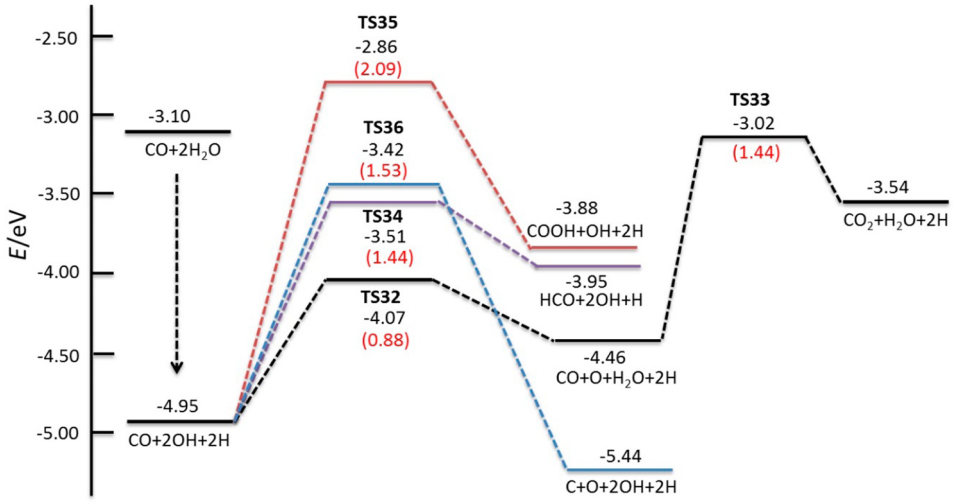

Figure 7. Potential energy surfaces of the reactions of CO and $2H_2O$ on the Fe(110) surface.

the back reactions reveals that CO_2 dissociation [$CO_2 \rightarrow CO + O$] is much favorable kinetically (0.35 eV) and thermodynamically (−1.45 eV), and the formed CO can be hydrogenated [$CO + H \rightarrow HCO$].

3.5. WGS Reaction on 0.25 ML H-Precovered Surface. Apart from the surface O and OH species, H is another inevitable surface species or the product of the WGS reaction. Therefore, we considered the reaction of CO and H_2O on the most stable 0.25 ML H-precovered Fe(110) surface.[70] The optimized structures of the stationary points of IS, TS, and FS are shown in Figure S7, and the structural parameters are listed in Table S7. The reaction barriers, the reaction energies, and the structural parameters of the TS are shown in Table S8. The total reaction potential energy surfaces are shown in Figure 6.

The coadsorption energy of CO and H_2O is −2.48 eV, which is higher than that (−2.33 eV) on the clean surface. On the basis of the coadsorbed CO + H_2O + 4H, the H_2O molecule adsorbs at the top site with the Fe−O distance of 2.146 Å, and CO adsorbs at the **3FH** site with the Fe−C distances of 1.922, 2.001, and 2.142 Å. There exists H-bonding between CO and H_2O (1.854 Å).

Although H_2O dissociative adsorption is more favorable, we computed HCO formation from CO hydrogenation at first. In the transition state **TS23**, the forming C−O distance is 1.376 Å. The energy barrier is 1.37 eV, and the reaction is endothermic by 1.13 eV. In addition, the adsorbed H_2O can dissociate into OH and H. In the transition state **TS24**, the breaking O−H distance is 1.442 Å. The energy barrier is 1.11 eV, and this reaction is exothermic by 0.66 eV. Therefore, H_2O dissociative adsorption is more favorable kinetically and thermodynamically. Following the H_2O dissociative adsorption, the subsequent CO hydrogenation has a barrier of 1.28 eV and is endothermic by 0.62 eV. In the transition state (**TS25**), the forming C−H distance is 1.342 Å. This reaction is easier to occur than that on the clean surface; i.e., the precovered H can promote CO hydrogenation.

Starting from the coadsorbed 4H + CO + OH + H, the subsequent OH dissociation needs a barrier of 1.00 eV and is exothermic by 0.41 eV. In the transition state **TS26**, the breaking O−H distance is 1.290 Å. For CO oxidation by surface O, the forming C−O distance in the transition state (**TS27**) is 1.698 Å. This reaction needs a barrier of 1.76 eV and is endothermic by 1.44 eV. Compared with CO oxidation on the clean surface, this reaction needs a higher barrier. We also calculated CO dissociation into C and O atoms. In the transition state (**TS28**), the breaking C−O distance is 1.810 Å. This reaction needs a barrier of 2.33 eV and is exothermic by 0.37 eV. Starting from the coadsorbed 4H + CO + OH + H, COOH formation has a barrier of 1.95 eV and is endothermic by 1.21 eV. In the transition state **TS29**, the forming C−O distance is 1.674 Å. This process is easier to occur than that on the clean surface (1.95 vs 2.11 eV).

The PES in Figure 6 shows clearly that, on the surface with coadsorbed CO + H_2O + 4H, the first step is H_2O dissociative adsorption, followed by HCO formation [4H + CO + $H_2O \rightarrow$ 4H + CO + OH + H → 4H + HCO + OH], while the formation of CO_2 and COOH is not favorable kinetically and thermodynamically. From the coadsorbed 4H + CO + H_2O to 4H + HCO + OH, the rate-determining step is CO hydrogenation to HCO via a barrier of 1.28 eV. The total reaction is exothermic by 0.04 eV. Compared with the clean surface, the precovered H atoms can lower the energy barrier of HCO formation (1.65 vs 1.28 eV) and make HCO formation from highly endothermic (0.88 eV) to slightly exothermic (−0.04 eV). Figure 6 shows also that CO_2 dissociation [$CO_2 \rightarrow CO + O$] is much favorable kinetically (0.33 eV) and thermodynamically (−1.44 eV), and the formed CO can be hydrogenated [$CO + H \rightarrow HCO$].

3.6. WGS Reaction on Different H_2O/CO Ratios. Apart from the clean surface as well as surfaces with the precoverage of O atoms, OH groups, and H atoms, we also became interested in the WGS reaction with different H_2O and CO ratios.

3.6.1. H_2O/CO = 2/1. In this section, we considered the WGS reaction of CO and $2H_2O$ through three routes: redox and COOH- and HCO-mediated mechanisms. The optimized structures of the stationary points of IS, TS, and FS are shown in Figure S8, and the structural parameters are listed in Table S9. The reaction barriers, the reaction energies, and the structural parameters of the TS are shown in Table S10. The total reaction potential energy surfaces are shown in Figure 7.

On the basis of the previous results[67] and the above discussion, the first step of the reaction is H_2O dissociation into surface O and H due to the low barriers and exothermic property. Starting from the coadsorbed CO + $2H_2O$, the dissociative adsorption energy of CO + 2OH + 2H is

DOI: 10.1021/acs.jpcc.5b07497
J. Phys. Chem. C 2015, 119, 28377−28388

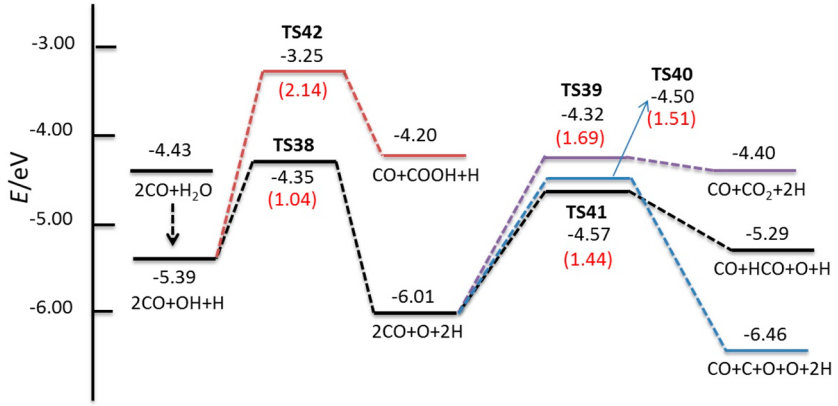

Figure 8. Potential energy surfaces of the reactions of 2CO and H_2O on the Fe(110) surface.

exothermic by 1.85 eV. For the redox mechanism [CO + 2OH + 2H → CO + O + H_2O + 2H → CO_2 + H_2O + 2H], the next step is the disproportionation reaction of 2OH into O + H_2O. In the transition state (**TS32**), the breaking and forming O−H distances are 1.095 and 1.384 Å, respectively. This step needs an activation barrier of 0.88 eV and is endothermic by 0.49 eV. In the final state (CO + O + H_2O + 2H), the H_2O molecule and O atom adsorb at the **T** and **LB** sites, respectively. The coadsorbed CO can be oxidized by the formed O atom. In the transition state (**TS33**), the forming C−O distance is 1.651 Å. This reaction has a barrier of 1.44 eV and is endothermic by 0.92 eV. As shown in Figure 7, CO_2 formation has an effective barrier of 1.93 eV and is endothermic by 1.41 eV.

For the HCO-mediated route [CO + 2OH + 2H → HCO + 2OH + H], the next step is the coupling of CO and H to form HCO. In the transition state **TS34**, the forming C−H distance is 1.325 Å. In this step, the barrier is 1.44 eV and the reaction is endothermic by 1.00 eV.

For the COOH-mediated mechanism [CO + 2OH + 2H → COOH + OH + 2H], the next step is the coupling of CO and OH starting from CO + 2OH + 2H. In the transition state **TS35**, the forming C−O distance is 1.839 Å. In this step, the barrier is 2.09 eV, and the reaction is endothermic by 1.07 eV. In addition, CO direct dissociation is also considered. In the transition state (**TS36**), the breaking C−O distance is 1.782 Å. This reaction needs a barrier of 1.53 eV and is exothermic by 0.49 eV.

The PES in Figure 7 shows clearly that the most favorable route is either CO dissociation or HCO formation, and both reactions have similar barriers (1.53 vs 1.44 eV); however, CO dissociation is much more favorable than HCO formation thermodynamically (−0.49 vs 1.00 eV). In contrast, the formation of COOH and CO_2 is much less favorable kinetically and thermodynamically. Figure 7 shows also that CO_2 dissociation [CO_2 → CO + O] is much favorable kinetically (0.52 eV) and thermodynamically (−0.92 eV), and the formed CO can be hydrogenated [CO + H → HCO].

3.6.2. H_2O/CO = 1/2. In this section, we considered the WGS reaction of 2CO and H_2O through three routes: redox and COOH- and HCO-mediated mechanisms. The optimized structures of the stationary points of IS, TS, and FS are shown in Figure S9, and the structural parameters are listed in Table S11. The reaction barriers, the reaction energies, and the structural parameters of the TS are shown in Table S12. The total PES is shown in Figure 8.

The coadsorption energy of 2CO + H_2O is −4.43 eV, which is only 0.07 eV higher than the total energies (−4.36 eV) of the individual adsorptions. In the coadsorption configuration, both H_2O and CO are at the top sites. In the first step, we computed H_2O dissociation. In the transition state **TS37**, the breaking O−H distance is 1.388 Å. The dissociation has a barrier of 0.91 eV and is exothermic by 0.96 eV. In the final state (2CO + OH + H), the OH and H adsorb at the **3FH** sites. The following step of the redox route [2CO + OH + H → 2CO + O + 2H → CO + CO_2 + 2H] is the dissociation of OH to O and H atoms. In the transition state (**TS38**), the breaking O−H distance is 1.294 Å. The barrier is 1.04 eV, and the reaction is exothermic by 0.62 eV. In the transition state of CO oxidation (**TS39**), the forming C−O distance is 1.590 Å. This reaction has barrier of 1.69 eV and is endothermic by 1.61 eV.

Alternatively, we computed CO dissociation and HCO formation from the coadsorbed 2CO + O + 2H. For CO dissociation, the breaking C−O distance in the transition state (**TS40**) is 1.772 Å. The barrier is 1.51 eV, and the reaction is exothermic by 0.45 eV. For HCO formation, the forming C−H distance in the transition state (**TS41**) is 1.447 Å. In this step, the barrier is 1.44 eV and the reaction is endothermic by 0.72 eV. In addition, COOH formation from the coadsorbed 2CO + OH + H has a barrier of 2.14 eV and is endothermic by 1.19 eV. In the transition state **TS42**, the forming C−O distance is 1.686 Å.

The PES in Figure 8 shows that the most favorable route is either CO dissociation or HCO formation, and both reactions have similar barriers (1.51 vs 1.44 eV); however, CO dissociation is much more favorable than HCO formation thermodynamically (−0.45 vs 0.72 eV). In contrast, the formation of COOH and CO_2 is much less favorable kinetically and thermodynamically. Figure 8 shows also the favorable CO_2 dissociation [CO_2 → CO + O]. The formed CO can be hydrogenated [CO + H → HCO].

3.7. Discussion. Having these results in hand, it is easy to analyze the reaction of CO and H_2O on different Fe(110) surfaces. On the clean surface with the coadsorbed CO + H_2O, CO dissociation and CO oxidation have similar barriers (1.58 and 1.61 eV, respectively); however, CO dissociation is much more favorable thermodynamically than CO oxidation (−0.41 vs 1.55 eV). This is because of the very strong difference in adsorption energy between the surface O atom deduced from H_2O dissociation [$H_2O_{(g)}$ = $2H_{(s)}$ + $O_{(s)}$] and CO_2 (−1.76 vs −0.54 eV). In contrast, the formation of COOH as well as HCO and COH is neither kinetically nor thermodynamically

DOI: 10.1021/acs.jpcc.5b07497
J. Phys. Chem. C 2015, 119, 28377−28388

favorable. Therefore, the clean Fe(110) surface does not promote the WGS reaction, while CO dissociation and CO oxidation are favorable.

With the precoverage of surface O atoms at 0.25 ML, the most favorable route is HCO formation. Compared with the clean surface, the barrier of HCO formation is lowered significantly (0.67 vs 1.65 eV), while that of CO dissociation is increased considerably (2.25 vs 1.61 eV). It is noted that O precoverage can lower the barrier of COOH formation (1.83 vs 2.11 eV), while it can enhance the barrier of CO oxidation (1.75 vs 1.61 eV). Therefore, O precoverage can promote HCO formation, while it can suppress CO oxidation and dissociation.

On the surface with OH precoverage at 0.25 ML, similar results as on the O-precovered surface have been found, i.e., favoring HCO formation and suppressing CO oxidation and dissociation. The barrier of HCO formation is much lower (1.26 eV) than those of CO dissociation and oxidation (2.47 and 1.80 eV, respectively). On the surface with H precoverage at 0.25 ML, the most favorable reaction route is also HCO formation with a barrier of 1.28 eV, while the barriers of CO dissociation and oxidation are much higher (1.76 and 2.33 eV, respectively).

On the H_2O-precovered surface (CO/H_2O = 1/2), CO dissociation and CO hydrogenation have similar barriers (1.53 vs 1.61 eV); however, CO dissociation is exothermic (−0.49 eV), while CO hydrogenation is endothermic (1.00 eV). In contrast, COOH formation and CO oxidation are not favorable kinetically and thermodynamically. Similar results are also found on the CO-precovered surface (CO/H_2O = 2/1); for example, the barriers of CO dissociation and CO hydrogenation are similar (1.51 vs 1.44 eV), and CO dissociation is exothermic (−0.45 eV), while CO hydrogenation is endothermic (0.72 eV).

Considering the back reaction, CO_2 dissociation is much favorable kinetically and thermodynamically on all of these surfaces. Compared with the reaction on the clean surface, some interesting points can be seen on the precovered surfaces. For example, CO_2 formation has similar barriers on O-, OH-, and H- as well as H_2O-precovered surfaces. However, the reaction energies become less endothermic, and this is because of the H-bonding interaction between the adsorbed CO_2 with other surface species. The same trend is also found for HCO, where the HCO formation is endothermic, while HCO dissociation becomes exothermic.

4. CONCLUSION

To understand the potential ability of the water-gas shift reaction catalyzed by metallic iron, we have carried out detailed density functional theory computation on the reactions of CO and H_2O on the clean Fe(110) surface as well as on the 0.25 ML O-, OH-, and H-precovered Fe(110) surfaces. We also have considered the reactions with different CO and H_2O ratios.

On all of these surfaces, H_2O dissociative adsorption [$H_2O \rightarrow OH + H \rightarrow O + 2H$] is very favorable kinetically and thermodynamically, and this is necessary for the redox reaction [$CO + O \rightarrow CO_2$] and the carboxylic reaction [$CO + OH \rightarrow COOH \rightarrow CO_2 + H$].

On the clean surface, CO oxidation following the redox mechanism has a similar barrier as CO dissociation; however, CO dissociation is much more favorable thermodynamically. In contrast, the formation of COOH as well as HCO and COH is neither kinetically nor thermodynamically favorable.

On the surface with O, OH, and H at 0.25 monolayer precoverage, CO hydrogenation is promoted, while CO oxidation and dissociation are suppressed.

On the surfaces with different CO and H_2O ratios, CO dissociation and CO hydrogenation have similar barriers; however, CO dissociation is exothermic, while CO hydrogenation is endothermic. On all of these surfaces, COOH formation is not favorable.

Considering the reverse reactions, CO_2 dissociation is much favorable kinetically and thermodynamically on all of these surfaces, and CO_2 can be hydrogenated easily.

On the basis of all of these results, it is concluded that metallic iron is not an appropriate catalyst for the water-gas shift reaction; instead, hydrocarbon formation should be likely.

■ ASSOCIATED CONTENT

Supporting Information

The Supporting Information is available free of charge on the ACS Publications website at DOI: 10.1021/acs.jpcc.5b07497.

Adsorption energies and bond distances of the IS, TS, and FS in the reaction of CO + H_2O (Tables S1, S3, S5, S7); barriers and reaction energies of the reaction of CO + H_2O, and the bond distances of the transition states (Tables S2, S4, S6, S8); adsorption energies and bond distances of the IS, TS, and FS in the reaction of CO + $2H_2O$ (Table S9); barriers and reaction energies of the reaction of CO + $2H_2O$, and the bond distances of the transition states (Table S10); adsorption energies and bond distances of the IS, TS, and FS in the reaction of 2CO + H_2O (Table S11); barriers and reaction energies of the reaction of 2CO + H_2O, and the bond distances of the transition states (Table S12); top and side views of the optimized geometries and adsorption energies for the stationary points in the reaction of CO + H_2O (Figures S1−S7); top and side views of the optimized geometries and adsorption energies for the stationary points in the reaction of CO + $2H_2O$ (Figure S8); and top and side views of the optimized geometries and adsorption energies for the stationary points in the reaction of 2CO + H_2O (Figure S9) (PDF)

■ AUTHOR INFORMATION

Corresponding Authors

*E-mail: ywl@sxicc.ac.cn (Y.-W.L.).
*E-mail: haijun.jiao@catalysis.de (H.J.).

Notes

The authors declare no competing financial interest.

■ ACKNOWLEDGMENTS

This work was supported by the National Basic Research Program of China (no. 2011CB201406), the National Natural Science Foundation of China (nos. 21273262 & 21273266), and the Chinese Academy of Science and Synfuels China. Co., Ltd. We also acknowledge general financial support from the BMBF and the state of Mecklenburg-Vorpommern.

■ REFERENCES

(1) Smith, R. J. B.; Loganathan, M.; Shantha, M. S. A Review of the Water Gas Shift Reaction Kinetics. *Int. J. Chem. React. Eng.* **2010**, *8*, 1542−6580.

DOI: 10.1021/acs.jpcc.5b07497
J. Phys. Chem. C 2015, 119, 28377−28388

(2) Newsome, D. S. The Water-Gas Shift Reaction. *Catal. Rev.: Sci. Eng.* **1980**, *21*, 275−318.
(3) Yeung, C. M. Y.; Yu, K. M. K.; Fu, Q. J.; Thompsett, D.; Petch, M. I.; Tsang, S. C. Engineering Pt in Ceria for a Maximum Metal-Support Interaction in Catalysis. *J. Am. Chem. Soc.* **2005**, *127*, 18010−18011.
(4) Hardacre, C.; Ormerod, R. M.; Lambert, R. M. Platinum-Promoted Catalysis by Ceria: A Study of Carbon Monoxide Oxidation over Pt(111)/CeO_2. *J. Phys. Chem.* **1994**, *98*, 10901−10905.
(5) Huang, S. C.; Lin, C. H.; Wang, J. H. Trends of Water Gas Shift Reaction on Closed-Packed Transition Metal Surfaces. *J. Phys. Chem. C* **2010**, *114*, 9826−9834.
(6) Grabow, L. C.; Gokhale, A. A.; Evans, S. T.; Dumesic, J. A.; Mavrikakis, M. Mechanism of the Water Gas Shift Reaction on Pt: First Priciples, Experiments, and Microkinetic Modeling. *J. Phys. Chem. C* **2008**, *112*, 4608−4617.
(7) Hilaire, S.; Wang, X.; Luo, T.; Gorte, R. J.; Wagner, J. A Comparative Study of Water-Gas-Shift Reaction over Ceria Supported Metallic Catalysts. *Appl. Catal., A* **2001**, *215*, 271−278.
(8) Jacobs, G.; Chenu, E.; Patterson, P. M.; Williams, L.; Sparks, D.; Thomas, G.; Davis, B. H. Water-Gas Shift: Comparative Screening of Metal Promoters for Metal/Ceria Systems and Role of the Metal. *Appl. Catal., A* **2004**, *258*, 203−214.
(9) Chen, Y. Y.; Dong, M.; Wang, J.; Jiao, H. On the Role of a Cobalt Promoter in a Water-Gas-Shift Reaction on Co-MoS_2. *J. Phys. Chem. C* **2010**, *114*, 16669−16676.
(10) Chen, Y. Y.; Dong, M.; Wang, J.; Jiao, H. Mechanisms and Energies of Water Gas Shift Reaction on Fe-, Co-, and Ni-Promoted MoS_2 Catalysts. *J. Phys. Chem. C* **2012**, *116*, 25368−25375.
(11) Wheeler, C.; Jhalani, A.; Klein, E. J.; Tummala, S.; Schmidt, L. D. The Water−Gas-Shift Reaction at Short Contact Times. *J. Catal.* **2004**, *223*, 191−199.
(12) Panagiotopoulou, P.; Kondarides, D. I. Effect of the Nature of the Support on the Catalytic Performance of Noble Metal Catalysts for the Water−Gas Shift Reaction. *Catal. Today* **2006**, *112*, 49−52.
(13) Panagiotopoulou, P.; Kondarides, D. I. Effect of Morphological Characteristics of TiO_2-Supported Noble Metal Catalysts on Their Activity for the Water-Gas Shift Reaction. *J. Catal.* **2004**, *225*, 327−336.
(14) Bunluesin, T.; Gorte, R. J.; Graham, G. W. Studies of the Water-Gas-Shift Reaction on Ceria-Supported Pt, Pd, and Rh: Implications for Oxygen-Storage Properties. *Appl. Catal., B* **1998**, *15*, 107−114.
(15) Wang, X.; Gorte, R. J.; Wagner, J. P. Deactivation Mechanisms for Pd/Ceria during the Water−Gas-Shift Reaction. *J. Catal.* **2002**, *212*, 225−230.
(16) Gorte, R. J.; Zhao, S. Studies of the Water-Gas-Shift Reaction with Ceria-Supported Precious Metals. *Catal. Today* **2005**, *104*, 18−24.
(17) Wang, X.; Gorte, R. J. The Effect of Fe and other Promoters on the Activity of Pd/Ceria for the Water-Gas Shift Reaction. *Appl. Catal., A* **2003**, *247*, 157−162.
(18) Jacobs, G.; Williams, L.; Graham, U.; Thomas, G. A.; Sparks, D. E.; Davis, B. H. Low Temperature Water−Gas Shift: in Situ DRIFTS-Reaction Study of Ceria Surface Area on the Evolution of Formates on Pt/CeO_2 Fuel Processing Catalysts for Fuel Cell Applications. *Appl. Catal., A* **2003**, *252*, 107−118.
(19) Tibiletti, D.; de Graaf, E. A. B.; Teh, S. P.; Rothenberg, G.; Farrusseng, D.; Mirodatos, C. Selective CO Oxidation in the Presence of Hydrogen: Fast Parallel Screening and Mechanistic Studies on Ceria-Based Catalysts. *J. Catal.* **2004**, *225*, 489−497.
(20) Tibiletti, D.; Goguet, A.; Meunier, F. C.; Breen, J. P.; Burch, R. On the Importance of Steady-State Isotopic Techniques for the Investigation of the Mechanism of the Reverse Water-Gas-Shift Reaction. *Chem. Commun.* **2004**, 1636−1637.
(21) Jacobs, G.; Patterson, P. M.; Graham, U. M.; Sparks, D. E.; Davis, B. H. Low Temperature Water-Gas Shift: Kinetic Isotope Effect Observed for Decomposition of Surface Formates for Pt/Ceria Catalysts. *Appl. Catal., A* **2004**, *269*, 63−73.
(22) Patt, J.; Moon, D. J.; Phillips, C.; Thompson, L. Molybdenum Carbide Catalysts for Water-Gas Shift. *Catal. Lett.* **2000**, *65*, 193−195.
(23) Moon, D. J.; Ryu, J. W. Molybdenum Carbide Water-Gas Shift Catalyst for Fuel Cell-Powered Vehicles Applications. *Catal. Lett.* **2004**, *92*, 17−24.
(24) Liu, P.; Rodriguez, J. A. Water-Gas-shift Reaction on Molybdenum Carbide Surfaces: Essential Role of the Oxycarbide. *J. Phys. Chem. B* **2006**, *110*, 19418−19425.
(25) Gokhale, A. A.; Dumesic, J. A.; Mavrikakis, M. On the Mechanism of Low-Temperature Water Gas Shift Reaction on Copper. *J. Am. Chem. Soc.* **2008**, *130*, 1402−1414.
(26) Ojifinni, R. A.; Froemming, N. S.; Gong, J. L.; Pan, M.; Kim, T. S.; White, J. M.; Henkelman, G.; Mullins, C. B. Water-Enhanced Low-Temperature CO Oxidation and Isotope Effects on Atomic Oxygen-Covered Au(111). *J. Am. Chem. Soc.* **2008**, *130*, 6801−6812.
(27) Rodriguez, J. A.; Ma, S.; Liu, P.; Hrbek, J.; Evans, J.; Pérez, M. Activity of CeO_x and TiO_x Nanoparticles Grown on Au(111) in the Water-Gas Shift Reaction. *Science* **2007**, *318*, 1757−1760.
(28) Wang, Y. Y.; Zhang, D. J.; Zhu, R. X.; Zhang, C. Q.; Liu, C. B. A Density Functional Theory Study of the Water-Gas Shift Reaction Promoted by Neutral, Anionic, and Cationic Gold Dimers. *J. Phys. Chem. C* **2009**, *113*, 6215−6220.
(29) Su, H.-Y.; Yang, M.-M.; Bao, X.-H.; Li, W.-X. The Effect of Water on the CO Oxidation on Ag(111) and Au(111) Surfaces: A First-Principle Study. *J. Phys. Chem. C* **2008**, *112*, 17303−17310.
(30) Rodriguez, J. A.; Liu, P.; Hrbek, J.; Evans, J.; Pérez, M. Water Gas Shift Reaction on Cu and Au Nanoparticles Supported on CeO_2(111) and ZnO(0001): Intrinsic Activity and Importance of Support Interactions. *Angew. Chem., Int. Ed.* **2007**, *46*, 1329−1332.
(31) Rodríguez, J. A.; Evans, J.; Graciani, J.; Park, J. B.; Liu, P.; Hrbek, J.; Sanz, J. F. High Water-Gas Shift Activity in TiO_2(110) Supported Cu and Au Nanoparticles: Role of the Oxide and Metal Particle Size. *J. Phys. Chem. C* **2009**, *113*, 7364−7370.
(32) Tang, Q. L.; Liu, Z. P. Identification of the Active Cu Phase in the Water-Gas Shift Reaction over Cu/ZrO_2 from First Principles. *J. Phys. Chem. C* **2010**, *114*, 8423−8430.
(33) Rodriguez, J. A.; Graciani, J.; Evans, J.; Park, J. B.; Yang, F.; Stacchiola, D.; Senanayake, S. D.; Ma, S.; Perez, M.; Liu, P.; Fdez Sanz, J.; Hrbek, J. Water-Gas Shift Reaction on a Highly Active Inverse CeO_x/Cu(111) Catalyst: Unique Role of Ceria Nanoparticles. *Angew. Chem., Int. Ed.* **2009**, *48*, 8047−8050.
(34) Park, J. B.; Graciani, J.; Evans, J.; Stacchiola, D.; Senanayake, S. D.; Barrio, L.; Liu, P.; Sanz, J. F.; Hrbek, J.; Rodriguez, J. A. Gold, Copper, and Platinum Nanoparticles Dispersed on CeO_x/TiO_2(110) Surfaces: High Water-Gas Shift Activity and the Nature of the Mixed-Metal Oxide at the Nanometer Level. *J. Am. Chem. Soc.* **2010**, *132*, 356−363.
(35) Shi, X. R.; Wang, S. G.; Hu, J.; Wang, H.; Chen, Y. Y.; Qin, Z. F.; Wang, J. G. Density Functional Theory Study on Water-Gas-Shift Reaction over Molybdenum Disulfide. *Appl. Catal., A* **2009**, *365*, 62−70.
(36) Oki, S.; Mezaki, R. Identification of Rate-Controlling Steps for the Water-Gas Shift Reaction over an Iron Oxide Catalyst. *J. Phys. Chem.* **1973**, *77*, 447−452.
(37) Rao, K. R. P. M.; Huggins, F. E.; Mahajan, V.; Huffman, G. P.; Rao, V. U. S. The Role of Magnetite in Fischer−Tropsch Synthesis. *Hyperfine Interact.* **1994**, *93*, 1745−1749.
(38) Keiski, R. L.; Salmi, T.; Niemistö, P.; Ainassaari, J.; Pohjola, V. J. Stationary and Transient Kinetics of the High Temperature Water-Gas Shift Reaction. *Appl. Catal., A* **1996**, *137*, 349−370.
(39) Joseph, Y.; Ranke, W.; Weiss, W. Water on FeO(111) and Fe_3O_4(111): Adsorption Behavior on Different Surface Terminations. *J. Phys. Chem. B* **2000**, *104*, 3224−3236.
(40) Rhodes, C.; Williams, B. P.; King, F.; Hutchings, G. J. Promotion of Fe_3O_4/Cr_2O_3 High Temperature Water Gas Shift Catalyst. *Catal. Commun.* **2002**, *3*, 381−384.
(41) Rhodes, C.; Hutchings, G. J. Studies of the Role of the Copper Promoter in the Iron Oxide/Chromia High Temperature Water Gas Shift Catalyst. *Phys. Chem. Chem. Phys.* **2003**, *5*, 2719−2723.

DOI: 10.1021/acs.jpcc.5b07497
J. Phys. Chem. C 2015, 119, 28377−28388

(42) Huang, D. M.; Cao, D. B.; Li, Y. W.; Jiao, H. Density Function Theory Study of CO Adsorption on Fe_3O_4(111) Surface. *J. Phys. Chem. B* **2006**, *110*, 13920−13925.
(43) Chen, L.; Ni, G.; Han, B.; Zhou, C. G.; Wu, J. P. Mechanism of Water Gas Shift Reaction on Fe_3O_4(111) Surface. *Acta Chim. Sin.* **2011**, *69*, 393−398.
(44) Rim, K. T.; Eom, D.; Chan, S. W.; Flytzani-Stephanopoulos, M.; Flynn, G. W.; Wen, X. D.; Batista, E. R. Scanning Tunneling Microscopy and Theoretical Study of Water Adsorption on Fe_3O_4: Implications for Catalysis. *J. Am. Chem. Soc.* **2012**, *134*, 18979−18985.
(45) Wang, X. J.; Renn, J.; Spencer, J.; Ratnasamy, C.; Cai, Y. A Novel Method for Measuring Active Sites of Fe_3O_4 for WGS Reaction. *Top. Catal.* **2013**, *56*, 1899−1905.
(46) Fu, Z. M.; Wang, J. Q.; Zhang, N.; An, Y. P.; Yang, Z. X. Effect of Cu Doping on the Catalytic Activity of Fe_3O_4 in Water-Gas Shift Reactions. *Int. J. Hydrogen Energy* **2015**, *40*, 2193−2198.
(47) Sun, Y.; Hla, S. S.; Duffy, G. J.; Cousins, A.; French, D.; Morpeth, L. D.; Edwards, J. H.; Roberts, D. G. Effect of Ce on the Structural Features and Catalytic Properties of La(0.9-x)CexFeO$_3$ Perovskite-like Catalysts for the High Temperature Water-Gas Shift Reaction. *Int. J. Hydrogen Energy* **2011**, *36*, 79−86.
(48) Lee, M. S.; Lee, J. Y.; Lee, D.-W.; Moon, D. J.; Lee, K.-Y. The Effect of Zn Addition into $NiFe_2O_4$ Catalyst for High-Temperature Shift Reaction of Natural Gas Reformate Assuming No External Steam Addition. *Int. J. Hydrogen Energy* **2012**, *37*, 11218−11226.
(49) Hallac, B. B.; Brown, J. C.; Baxter, L. L.; Argyle, M. D. A Kinetic Study on the Structural and Functional Roles of Lanthana in Iron-Based High Temperature Water-Gas Shift Catalysts. *Int. J. Hydrogen Energy* **2014**, *39*, 7306−7317.
(50) Reddy, G. K.; Smirniotis, P. G. Effect of Copper as a Dopant on the Water Gas Shift Activity of Fe/Ce and Fe/Cr Modified Ferrites. *Catal. Lett.* **2011**, *141*, 27−32.
(51) Niemantsverdriet, J. W.; Van der Kraan, A. M.; van Dijk, W. L.; van der Baan, H. S. Behavior of Metallic Iron Catalysts during Fischer−Tropsch Synthesis Studied with Mössbauer Spectroscopy, X-ray Diffraction, Carbon Content Determination, and Reaction Kinetic Measurements. *J. Phys. Chem.* **1980**, *84*, 3363−3370.
(52) Dry, M. E. The Sasol Route to Fuels. *Chemtech.* **1982**, *12*, 744−750.
(53) Dictor, R. A.; Bell, A. T. Fischer−Tropsch synthesis over reduced and unreduced iron oxide catalysts. *J. Catal.* **1986**, *97*, 121−136.
(54) Eliason, S. A.; Bartholomew, C. H. Reaction and Deactivation Kinetics for Fischer−Tropsch Synthesis on Unpromoted and Potassium-Promoted Iron Catalysts. *Appl. Catal., A* **1999**, *186*, 229−243.
(55) Lohitharn, N.; Goodwin, J. G., Jr.; Lotero, E. Fe-based Fischer−Tropsch Synthesis Catalysts Containing Carbide-Forming Transition Metal Promoters. *J. Catal.* **2008**, *255*, 104−113.
(56) Ojeda, M.; Nabar, R.; Nilekar, A. U.; Ishikawa, A.; Mavrikakis, M.; Iglesia, E. CO Activation Pathways and the Mechanism of Fischer−Tropsch Synthesis. *J. Catal.* **2010**, *272*, 287−297.
(57) Kresse, G.; Furthmüller, J. Efficiency of Ab-initio Total Energy Calculations for Metals and Semiconductors Using A Plane-wave Basis Set. *Comput. Mater. Sci.* **1996**, *6*, 15−50.
(58) Kresse, G.; Furthmüller, J. Efficient Iterative Schemes for Ab Initio Total-energy Calculations Using A Plane-wave Basis Set. *Phys. Rev. B: Condens. Matter Mater. Phys.* **1996**, *54*, 11169−11186.
(59) Blöchl, P. E. Projector Augmented-Wave Method. *Phys. Rev. B: Condens. Matter Mater. Phys.* **1994**, *50*, 17953−17979.
(60) Kresse, G.; Joubert, D. From Ultrasoft Pseudopotentials to the Projector Augmented-Wave Method. *Phys. Rev. B: Condens. Matter Mater. Phys.* **1999**, *59*, 1758−1775.
(61) Perdew, J. P.; Burke, K.; Ernzerhof, M. Generalized Gradient Approximation Made Simple. *Phys. Rev. Lett.* **1996**, *77*, 3865−3868.
(62) Henkelman, G.; Uberuaga, B. P.; Jónsson, H. A Climbing Image Nudged Elastic Band Method for Finding Saddle Points and Minimum Energy Paths. *J. Chem. Phys.* **2000**, *113*, 9901−9904.
(63) Monkhorst, H. J.; Pack, J. D. Special Points for Brillouin-Zone Integrations. *Phys. Rev. B* **1976**, *13*, 5188−5192.
(64) Kohlhaas, R.; Donner, P.; Schmitz-Pranghe, N. The Temperature Dependence of the Lattice Parameters of Iron, Cobalt, and Nickel in the High-temperature Range. *Z. Angew. Phys.* **1967**, *23*, 245.
(65) Kittel, C. *Introduction to Solid State Physics*, 7th ed.; Wiley: New York, 1996.
(66) Liu, S. L.; Tian, X. X.; Wang, T.; Wen, X. D.; Li, Y.-W.; Wang, J.; Jiao, H. High Coverage Water Aggregation and Dissociation on Fe(100): A Computational Analysis. *J. Phys. Chem. C* **2014**, *118*, 26139−26154.
(67) Liu, S. L.; Tian, X. X.; Wang, T.; Wen, X. D.; Li, Y.-W.; Wang, J.; Jiao, H. Coverage Dependent Water Dissociative Adsorption on Fe(110) from DFT Computation. *Phys. Chem. Chem. Phys.* **2015**, *17*, 8811−8821.
(68) Liu, S. L.; Tian, X. X.; Wang, T.; Wen, X. D.; Li, Y.-W.; Wang, J.; Jiao, H. Coverage Dependent Water Dissociative Adsorption on the Clean and O-pre-covered Fe(111) Surfaces. *J. Phys. Chem. C* **2015**, *119*, 11714−11724.
(69) Gao, R.; Cao, D.-B.; Liu, S.; Yang, Y.; Li, Y.-W.; Wang, J.; Jiao, H. Density Functional Theory Study into H_2O Dissociative Adsorption on the Fe_5C_2(010) Surface. *Appl. Catal., A* **2013**, *468*, 370−383.
(70) Wang, T.; Wang, S.; Luo, Q.; Li, Y.-W.; Wang, J.; Beller, M.; Jiao, H. Hydrogen Adsorption Structures and Energetics on Iron Surfaces at High Coverage. *J. Phys. Chem. C* **2014**, *118*, 4181−4188.
(71) Wang, T.; Tian, X.-X.; Li, Y.-W.; Wang, J.; Beller, M.; Jiao, H. High Coverage CO Activation Mechanisms on Fe(100) from Computations. *J. Phys. Chem. C* **2014**, *118*, 1095−1101.
(72) Huo, C. F.; Wu, B. S.; Gao, P.; Yang, Y.; Li, Y. W.; Jiao, H. The Mechanism of Potassium Promoter: Enhancing the Stability of Active Surfaces. *Angew. Chem., Int. Ed.* **2011**, *50*, 7403−7406.
(73) Wang, T.; Tian, X.-X.; Li, Y.-W.; Wang, J.; Beller, M.; Jiao, H. Coverage Dependent CO Adsorption and Activation Mechanisms on Iron Surfaces from DFT Computations. *ACS Catal.* **2014**, *4*, 1991−2005.
(74) Stibor, A.; Kresse, G.; Eichler, A.; Hafner, J. Density Functional Study of the Adsorption of CO on Fe(110). *Surf. Sci.* **2002**, *507*−*510*, 99−102.
(75) Jiang, D. E.; Carter, E. A. Adsorption and Dissociation of CO on Fe(110) from First Principles. *Surf. Sci.* **2004**, *570*, 167−177.
(76) Sun, X.; Forster, S.; Li, Q. X.; Kurahashi, M.; Suzuki, T.; Zhang, J. W.; Yamauchi, Y.; Baum, G.; Steidl, H. Spin-Polarization Study of CO Molecules Adsorbed on Fe(110) using Metastable-Atom Deexcitation Spectroscopy and First-Principles Calculations. *Phys. Rev. B: Condens. Matter Mater. Phys.* **2007**, *75*, 035419.
(77) Sorescu, D. C. Plane-Wave DFT Investigations of Adsorption, Diffusion, and Activation of CO on Kinked Fe(710) and Fe(310) Surfaces. *J. Phys. Chem. C* **2008**, *112*, 10472−10489.
(78) Wang, S. G.; Liao, X. Y.; Cao, D. B.; Huo, C. F.; Li, Y.-W.; Wang, J.; Jiao, H. Factors Controlling the Interaction of CO_2 with Transition Metal Surfaces. *J. Phys. Chem. C* **2007**, *111*, 16934−16940.
(79) Behner, H.; Spiess, W.; Wedler, G.; Borgmann, D. Interaction of Carbon Dioxide with Fe(110), Stepped Fe(110) and Fe(111). *Surf. Sci.* **1986**, *175*, 276−286.
(80) Dwyer, D. J.; Kelemen, S. R.; Kaldor, A. The Water Dissociation Reaction on Clean and Oxidized Iron (110). *J. Chem. Phys.* **1982**, *76*, 1832−1837.

DOI: 10.1021/acs.jpcc.5b07497
J. Phys. Chem. C 2015, 119, 28377−28388